RSC Advances

PAPER

View Article Online
View Journal | View Issue

Cite this: *RSC Adv.*, 2024, **14**, 19312

Preparation of an injectable zinc-containing hydrogel with double dynamic bond and its potential application in the treatment of periodontitis

Mei Yang, Dejiang Du, Yuanping Hao, Zhaojian Meng, Haiyu Zhang and Yuhan Liu *

Periodontal tissue regeneration continues to face significant clinical challenges. Periodontitis leads to alveolar bone resorption and even tooth loss due to persistent microbial infection and persistent inflammatory response. As a promising topical drug delivery system, the application of hydrogels in the controlled release of periodontal bioactive drugs has aroused great interest. Therefore, the design and preparation of an injectable hydrogel with self-repairing properties for periodontitis treatment is still in great demand. In this study, polysaccharide-based self-healing hydrogels with antimicrobial osteogenic properties were developed. Zinc ions are introduced into a dynamic cross-linking network formed by dynamic Schiff bases between carboxymethyl chitosan and oxidized hyaluronic acid *via* coordination bonds. The OC–Zn hydrogels exhibited good tissue adhesion, good fatigue resistance, excellent self-healing ability, low cytotoxicity, good broad-spectrum antimicrobial activity, and osteogenic activity. Therefore, the designed hydrogels allow the development of drug delivery systems as a potential treatment for periodontitis.

Received 22nd January 2024
Accepted 1st June 2024

DOI: 10.1039/d4ra00546e

rsc.li/rsc-advances

Introduction

Periodontitis is an inflammatory disease caused by a biofilm that leads to loss of gingival attachment, periodontal pocket formation, and alveolar bone resorption, which may eventually progress to tooth loss if left untreated.[1] Periodontitis is one of the most common dental diseases, affecting 90% of the global population, and is strongly associated with chronic non-communicable diseases such as cerebrovascular disease, coronary heart disease, cardiovascular disease, and cancer.[2,3] Long-term, effective control of infection and inflammation is the key to the treatment of periodontitis. Traditionally, mechanical debridement combined with adjunctive antibiotic therapy has been considered the mainstay of treatment for periodontal disease and imposes a heavy financial burden on patients.[4,5] However, due to the complex anatomy of periodontal pockets and antibiotic resistance, it is almost difficult to completely remove microorganisms and pathogens deep inside the periodontal pockets using conventional treatments.[6] It has been reported that 74.2% of patients with chronic periodontitis show subgingival pathogens resistant to one or more of the experimental antibiotics, and these challenges will limit the therapeutic outcomes and the future application of antibiotic-based topical drug delivery systems.[7] To overcome these challenges, extensive research has been devoted to the development of novel topical antimicrobial systems to improve the therapeutic outcome of periodontitis.[8,9]

Hydrogels, with good hydrophilicity and three-dimensional porous structure, are an ideal platform for periodontal drug delivery.[10–13] Compared to pre-formed scaffolds, injectable hydrogels are administered in a minimally invasive manner, which is ideal for irregularly shaped areas and reduces the risk of infection.[14,15] The hydrogel is injected into the periodontal pocket and then cured *in situ*. Self-healing hydrogels are triggered by the inherent regenerative capacity of natural tissues that develop through dynamic covalent bonding and non-covalent interactions.[16,17] Self-healing hydrogels can self-repair after minor injuries and maintain structural integrity in a timely manner, facilitating drug delivery in dynamic environments.[18–20]

Chitosan (CS) is a biocompatible and cationic polysaccharide with intrinsic antimicrobial activity by binding to negatively charged bacterial cell membranes or biomolecules, disrupting cell membranes and metabolism.[21] Carboxymethyl chitosan (CMCS), as a water-soluble derivative of CS, is a promising candidate for treating periodontal diseases due to its excellent antimicrobial properties, biodegradability, and biocompatibility.[22] In addition, hyaluronic acid (HA), another polysaccharide commonly found in the extracellular matrix,

Qingdao Stomatological Hospital Affiliated to Qingdao University, Qingdao 266000, Shandong, China

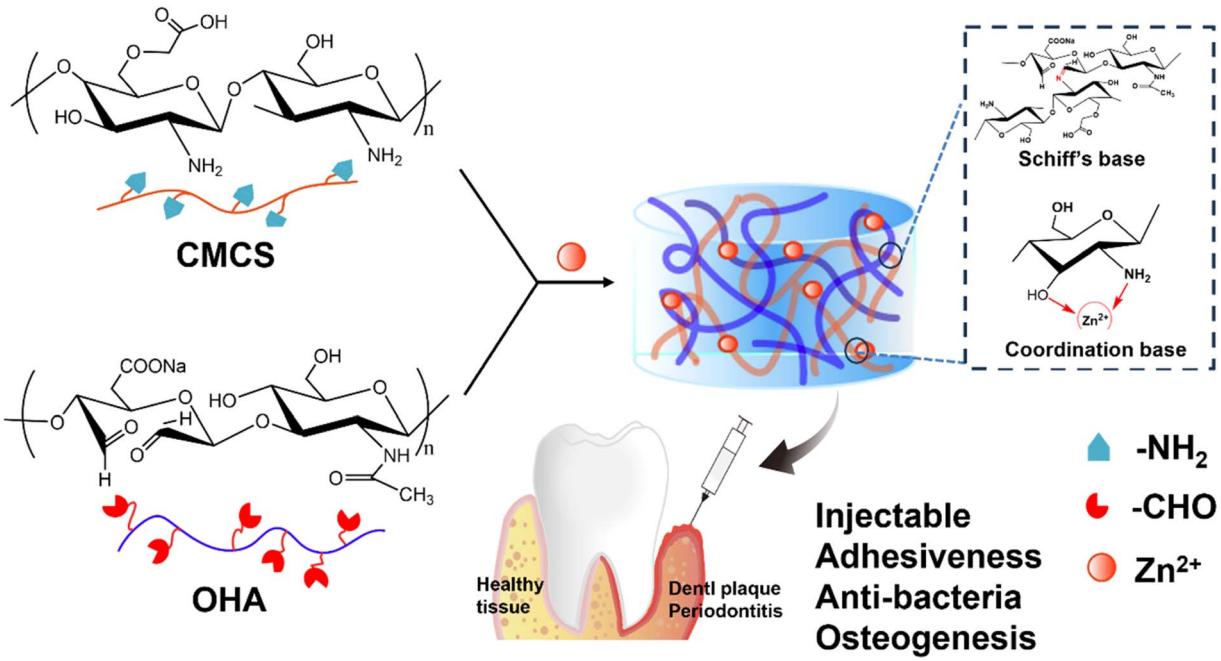

Scheme 1 Schematic of the fabrication route of multifunctional OC–Zn hydrogels with the potential for periodontitis.

accumulates at the wound site during the healing process.[23] It regulates cellular function by interacting directly with receptors on the cell membrane or indirectly with cytokines in the extracellular matrix.[24] Metal ions have been used as a therapeutic agent for various biomedical applications due to their availability, low cost, stability, and enhanced safety.[25] Among metal ions, zinc is a micronutrient that aids in wound healing and inhibits bacterial growth during the healing process.[26] To the best of our knowledge, there are no studies on the synthesis and characterization of self-healing hydrogels based on CMCS, aldehyde–hyaluronic acid, and zinc.

This study aimed to develop and evaluate self-healing hydrogels for periodontal disease. We constructed a drug-free polysaccharide-based injectable hydrogel (OC–Zn) through dynamic imine bonding and electrostatic interactions between CMCS and OHA, as well as ligand bonding between zinc ions, as shown in Scheme 1. The synthesized OC–Zn hydrogel showed synergistic therapeutic potential to promote periodontal tissue regeneration by killing pathogenic bacteria and modulating the osteogenic microenvironment. The structural and physicochemical properties of OC–Zn hydrogels were systematically characterized in terms of microstructure, gelation time, swelling behavior, rheological and self-healing behavior, mechanical properties, and tissue adhesion. In addition, the hemocompatibility and cytotoxicity, *in vitro* antimicrobial activity, and osteogenesis-promoting performance of OC–Zn hydrogels were also evaluated.

Results and discussion

Preparation and characterization of the OC–Zn hydrogels

To address the multiple needs of periodontal treatment, a self-healing, antibacterial, and osteogenic hydrogel was designed herein. The preparation diagram of the injectable hydrogel comprised of OHA, CMCS, and $ZnCl_2$ is displayed in Scheme 1. Aldehyde-decorated hyaluronate was synthesized through the oxidation of hyaluronate in the presence of sodium periodate and the structure was confirmed by ^{1}H NMR and FTIR spectrum (Fig. 1).[13,27] The ^{1}H NMR spectrum of OHA displayed a triplet peak near 4.93, 5.02 and 5.15 ppm corresponding to the ATR-FTIR absorption region of 1732 cm^{-1}, which indicates the format of hydrogen on the skeleton of the open-loop D-glucuronic acid unit in HA due to the stretching vibration of the –C=O bond in the aldehyde. These results confirm the successful synthesis of OHA. Hydrogels can be quickly formed at 37 °C *via* multiple crosslinking, including the electrostatic interactions between macromolecular chains, Zn–O, Zn–N coordination, and a Schiff's base reaction between the amino group from CMCS and the aldehyde group from OHA.[22,28] Fig. 1B shows the sol–gel process of OC–Zn hydrogel where the OC–Zn hydrogel was successfully formed. Besides, the OC–Zn hydrogel can instantly recover to its original state without any damage after compression. Additionally, the OC–Zn series hydrogels were further characterized by Fourier-transform infrared (FTIR), and the results a new characteristic peak of 1607 cm^{-1} for the dynamic Schiff base (imine) C=N bond with the disappearance of the aldehyde groups in OHA, which confirmed the successful preparation of OC–Zn hydrogel. Besides, scanning electron microscope (SEM) exhibited OC–Zn hydrogels have a homogeneous microporous structure and the internal pore size of the hydrogel decreased after increasing Zn^{2+} concentrations, which may be attributable to the good crosslinking between OHA, CMCS *via* Schiff-based bond and Zn–O, Zn–N coordination and simultaneous interactions.

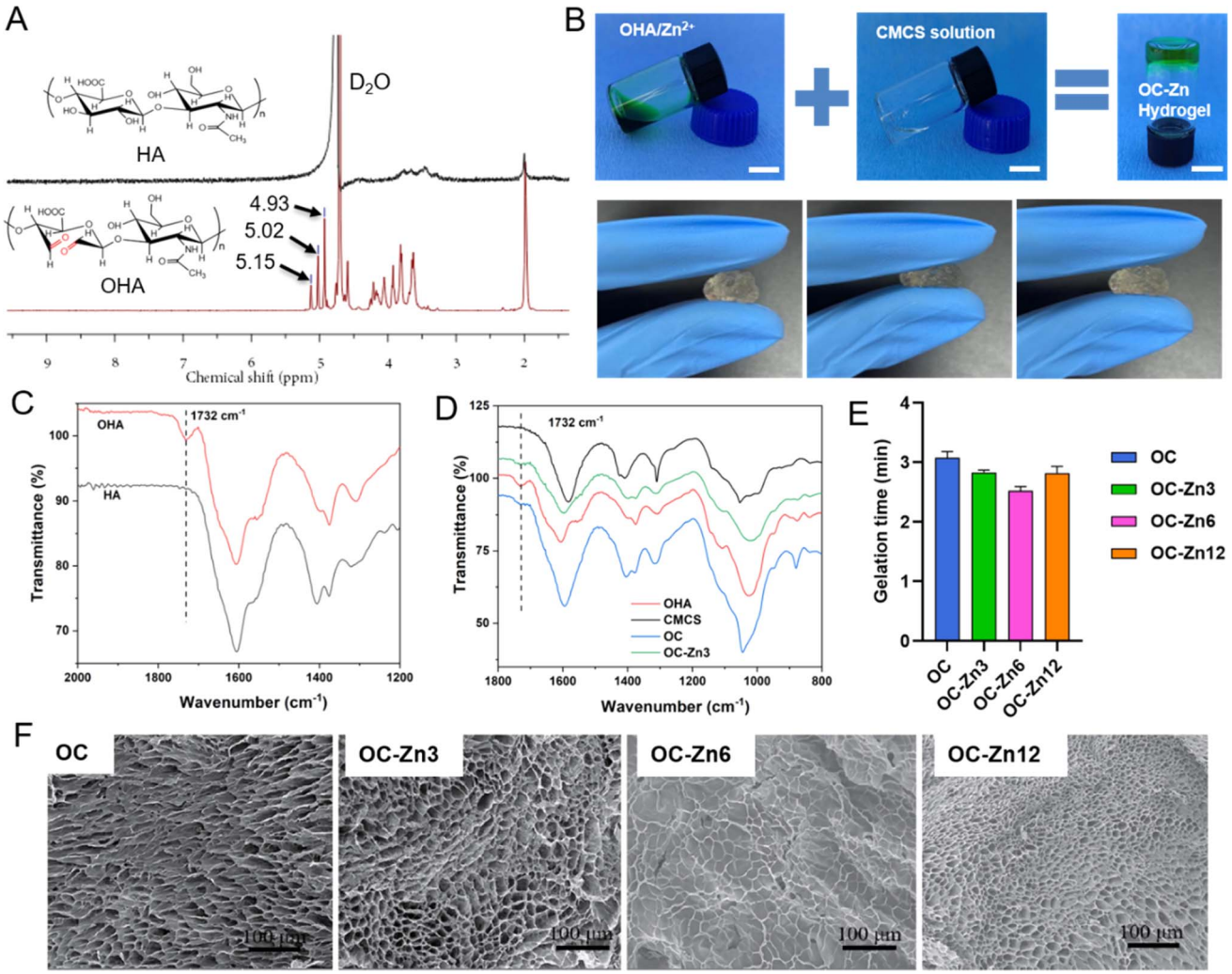

Fig. 1 (A) ^{1}H NMR spectra of HA and OHA. (B) Photograph displaying the mixing of OHA/Zn^{2+} and CMCS to form OC–Zn hydrogel, as well as the compression process of OC–Zn hydrogel (scale bar: 1 cm). (C) and (D) FT-IR spectra of HA, OHA, OC and OC–Zn hydrogels. Gelation time (E), representative SEM images (F) of OC and OC–Zn hydrogels. OC–Zn3, OC–Zn6, and OC–Zn12 represent hydrogels with final $ZnCl_2$ concentrations of 0.03, 0.06, and 0.12% (w/v), respectively.

Evaluation of the injectable self-healing behavior, rheology, swelling, adhesiveness performance of the OC–Zn hydrogels

To demonstrate that OC–Zn hydrogels can maintain the periodontal microenvironment, it is vital that we confirm their injectable self-healing behavior, rheology, adhesiveness, and swelling performance. First, the injectable self-healing properties of the hydrogel are proven. As shown in Fig. 2A, OC–Zn hydrogel could be injected into the shape of teeth and "QSH" through commonly used-gauge needles, and subsequently re-obtained their original shape integrity post-injection. The excellent injectable properties of OC–Zn hydrogels will benefit greatly from later *in situ* injection filling of periodontal pockets, where they can be applied to irregular shapes.

As hydrogel is administered for periodontal tissues, their great architecture stability after the swelling is crucial. The swelling ratio of freeze-dried samples in PBS as the concentration of Zn increased. Meanwhile, the degradation behavior was also observed, and the hydrogels could maintain the original integral shape within 24 h (Fig. 2B). Due to external forces such as oral chewing and the semi-enclosed anatomical position of the periodontal tissue, hydrogels' mechanical properties (*e.g.*, recoverability, deformability, *etc.*) are particularly important.[10,29] As a promising candidate for periodontal use, OC–Zn hydrogels formed by multiple dynamic cross-linking had satisfactory mechanical properties, including excellent recoverability and deformability.[30] Rheological measurements were performed on the OC–Zn hydrogels to explore their mechanical properties. Here, the elasticity and flowability were evaluated in terms of storage modulus and loss modulus, termed G′ and G″, respectively. As shown in Fig. 2C, all the tested groups of hydrogels exhibited elastic behavior, with G′ being greater than G″. To evaluate the self-healing ability of OC–Zn hydrogel, the samples that were stained with red and green pigments were split in half and then recombined into the differently stained parts. After 20 min, the integrated hydrogels could lift under self-weight (Fig. 2E). The results indicated that the OC–Zn hydrogels

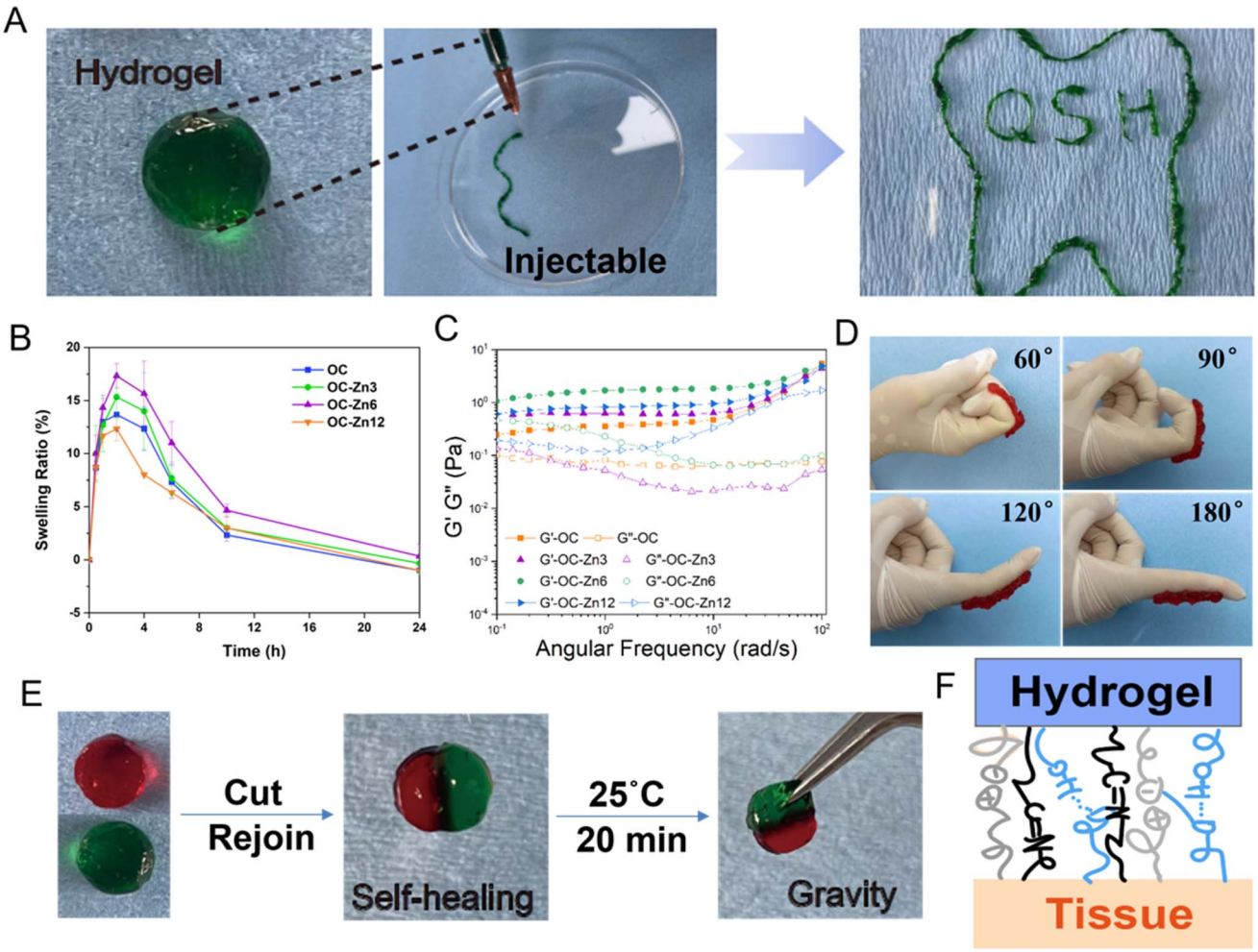

Fig. 2 (A) Image of the injectable of OC–Zn hydrogel into various shapes. (B) Swelling ratio and degradation trend of the OC–Zn hydrogels at the pH of 7.4. (C) Rheology characterizations (G′, G″) of OC, OC–Zn3, OC–Zn6, and OC–Zn12 hydrogels. (D) The OC–Zn hydrogel adapting to the movement of the finger joint. (E) Self-healing property of OC–Zn3 hydrogel. (F) Hydrogel adhesion mechanism.

could rapidly self-heal even after damage, prevent mechanical damage, and maintain the stability of periodontal tissue delivery under oral movement. We proposed that the Schiff base bonds between the $-NH_2$ of CMCS and –CHO of OHA and the coordination bond between zinc ion and O, N undergo dynamic cross-linking to achieve self-healing.[28] As exhibited in Fig. 2D, OC–Zn hydrogel can be rotated arbitrarily on the model's finger without shedding and shows good fatigue resistance in 10 bending cycles. The repeated bending and extension of the finger did not affect its adhesion ability. This hydrogel could produce instant tissue-material interfacial interactions with the tissue through multiple forces, including electrostatic interactions, hydrogen bonding, and Schiff base bonding (Fig. 2F).

Evaluation of the biocompatibility of the OC–Zn hydrogels

Good biocompatibility is an essential factor for biomaterials.[27,31] Here, the *in vitro* hemolysis test was performed to estimate the hemocompatibility of the OC–Zn hydrogels. Fig. 3A shows the distinct differences in color between the four hydrogel groups, the negative control (NS) and the positive control (Triton X-100). All four hydrogel groups were colorless and transparent, similar to the negative control, while the deionized water group was bright red. From the quantitative data in Fig. 3A, the hemolysis rate of the OC–Zn hydrogel was extremely low compared to the OC hydrogel (~1.3%), indicating that the hemolysis rate was significantly reduced by the addition of zinc ions. Furthermore, hPDLSCs and MC3T3 cells were used to evaluate the cytocompatibility through the cytoskeleton/nuclear and cell counting kit-8 (CCK8) assays. As shown in Fig. 3C, the morphology of the cytoskeleton and nucleus in the hydrogel groups presented normal structural characteristics like those of the control group. The CCK8 assay examined the cell proliferation rate in the hydrogel extract. The cell vitality in OC–Zn12 group was significantly lower than that of the other groups at 1 day and 3 days. Nonetheless, no significant difference was observed in the proliferation rate of each hydrogel group compared to the control at 5 days. Overall, all experiments confirmed that the OC–Zn hydrogels had excellent biocompatibility.

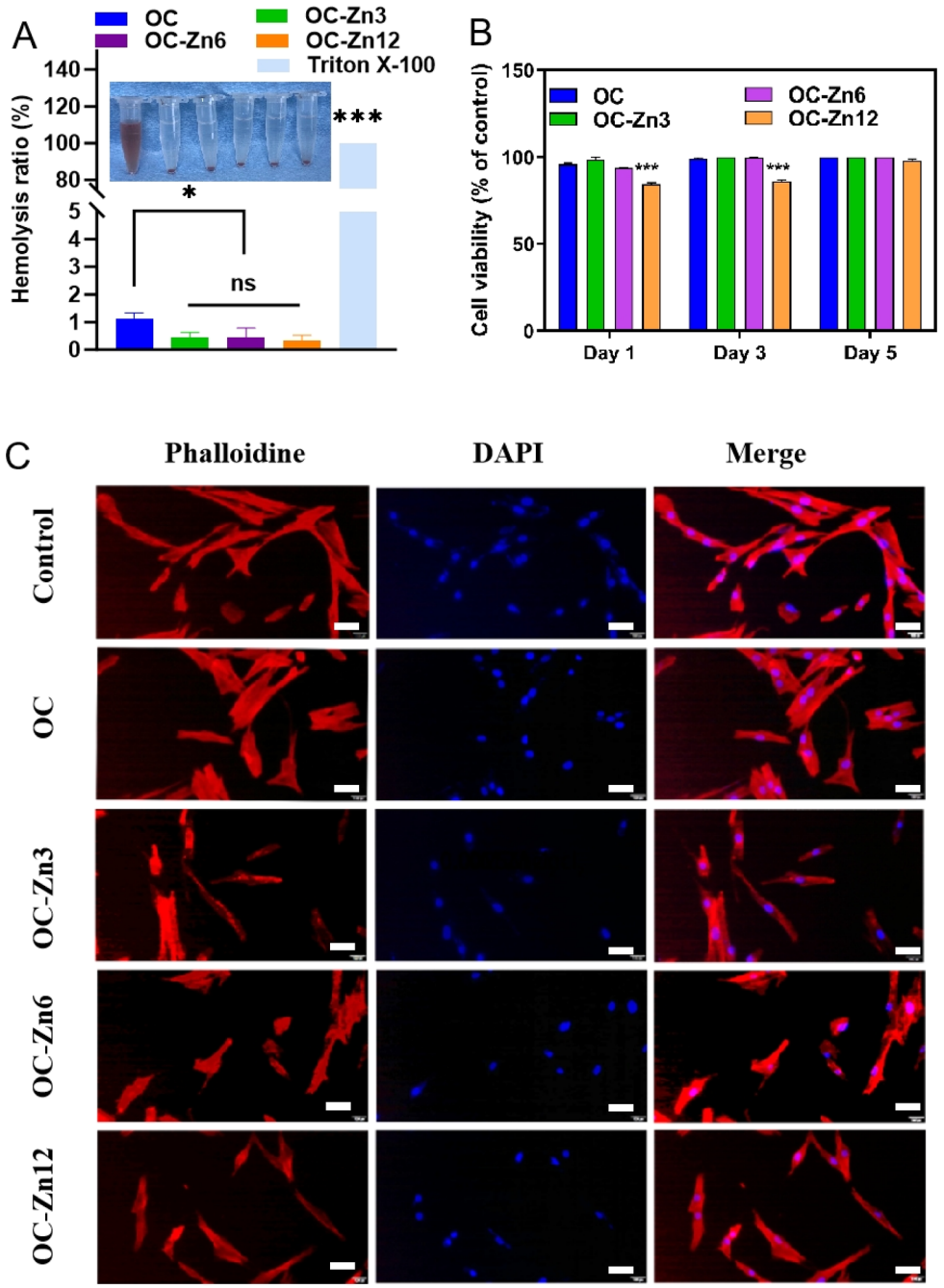

Fig. 3 (A) Hemolysis ratio of hydrogels. (B) Cell viability of MC3T3 cells after 1, 3, and 5 days of incubation with hydrogels (*: $p < 0.05$; ***: $p < 0.001$). (C) Fluorescence images of hPDLSCs treated with the hydrogels (scale bar: 100 μm).

Evaluation of the anti-bacterial activity of the OC–Zn hydrogels

Microbial infections are an extremely distressing problem that can accelerate alveolar bone degeneration and aggravate periodontal disease.[32,33] Two common pathogens – *Fusobacterium nucleatum* (*F. nucleatum*) and *Staphylococcus aureus* (*S. aureus*) in periodontal pockets were used as representative pathogenic bacteria to evaluate the antibacterial activity of these hydrogels. The microbial proliferation was assessed by colony assay.[34] The images of the spread plates of *F. nucleatum* and *S. aureus* disclosed a lower bacterial count in the hydrogel groups compared to the control group, and the bactericidal effect was significantly enhanced with increasing zinc ion concentration ($p < 0.05$). In the time kill assay (Fig. 4C, $p < 0.05$), it can be seen that the antibacterial ability of hydrogel increases with the increase of time, which may be due to the slow release of components in hydrogel. CMCS is one of the main antibacterial active ingredients of hydrogels. The pristine OC hydrogel (without $ZnCl_2$) exhibits good antimicrobial capacity by continuously releasing cations to disrupt bacterial cell walls and

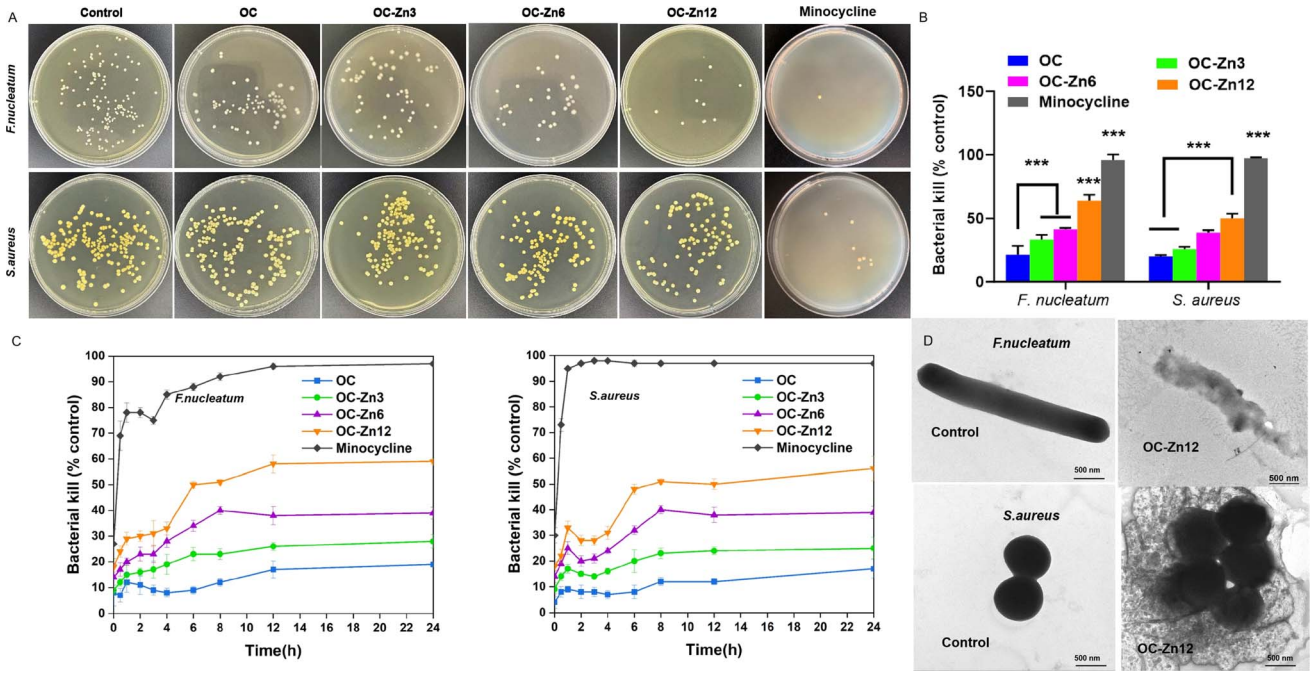

Fig. 4 Antibacterial activity evaluation of prepared hydrogels. (A) Representative photographs (10^6-fold dilution) and (B) quantitative results of survival bacteria colonies on agar plates after incubating the bacterial suspension with the prepared hydrogels (***: $p < 0.001$). (C) Quantitative results of survival bacteria colonies on agar plates after incubating the bacterial suspension with the prepared hydrogels within 24 h. (D) TEM images of bacterial morphology of control group and treated with OC–Zn12 hydrogel.

boost cell membrane permeability, leading to the lysis of the bacteria and the exudation of cell contents.[35,36] On the other hand, zinc ions might generate reactive oxygen species (ROS) in cells, induce gene expression related to oxidative stress, inhibit the synthesis of the cell wall, and thus result in microbial growth inhibition and death.[37,38] The integrity of the bacterial wall was further detected using TEM. As depicted in Fig. 4D, the bacteria in the control group showed a typical shaped

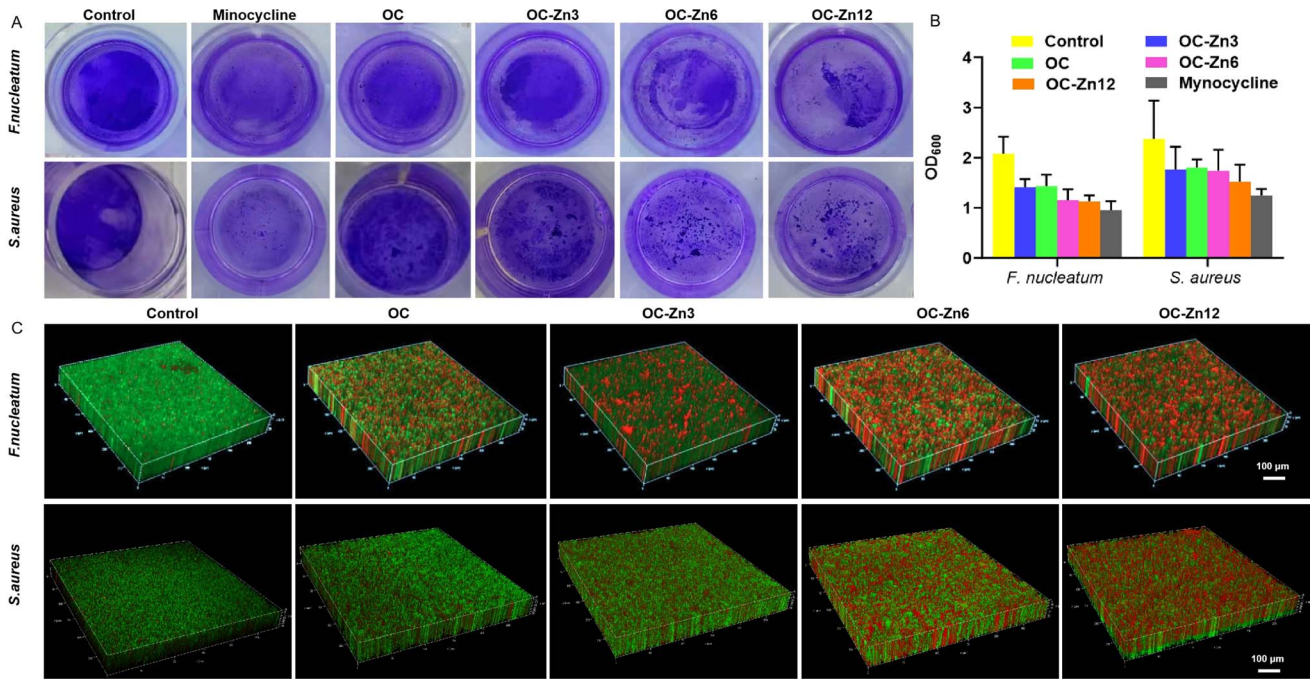

Fig. 5 Anti-biofilm activity evaluation of prepared hydrogels. (A) Representative crystal violet staining images of biofilm treated with different hydrogels and (B) the biofilm biomass ($n = 3$). (C) CLSM images of *F. nucleatum* and *S. aureus* biofilms grown for 48 h and treated with hydrogels for 12 h. Green is live cells. Red is dead cells.

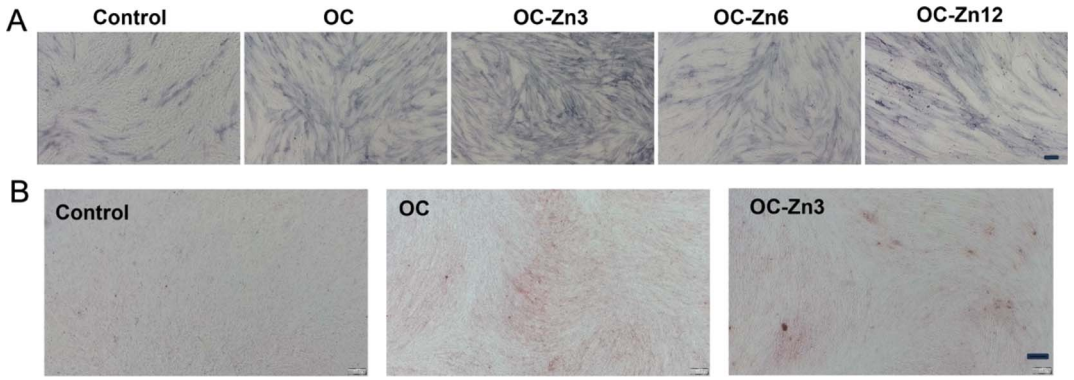

Fig. 6 (A) ALP staining of hPDLSCs on day 7 (scale bar: 100 μm). (B) ARS staining on day 21 (scale bar: 100 μm).

morphology with integrated cell walls. As we suspected, after OC–Zn12 treatment, the bacterial surface disintegrated into the fuzzy boundary. Thus, these results imply that cellular leakage caused by bacterial wall disruption may be one of the antimicrobial mechanisms of the prepared hydrogel. Therefore, the high antibacterial efficiency of OC–Zn hydrogels may be due to the synergistic attributes of both CMCS and zinc ions.

Evaluation of the anti-biofilm activity of the OC–Zn hydrogels

Biofilms composed of microorganisms and extracellular polymeric substances (EPS) can induce persistent bacterial infections.[39,40] First, the biomass of biofilm after different treatments was quantitatively determined by crystal violet staining. As shown in Fig. 5A/B, all hydrogel groups had different degrees of anti-biofilm effect, but there was no significant difference between groups. To investigate the effect of hydrogels on bacterial biofilms, biofilms cultured for 48 h were treated with the prepared hydrogels for 12 h. The biofilms were stained with live/dead fluorescence kits, and the disruptive effect was observed with CLSM.[41,42] As shown in Fig. 5C, the CLSM image showed that the blank group was covered by biofilm. Importantly, with the increase of zinc ion concentration, the number of dead red bacteria embedded in the biofilm increased, demonstrating the good biofilm eradication capacity of the hydrogel.

Evaluation of the OC–Zn hydrogels

ALP staining and alizarin red staining (ARS) were used to detect the osteogenic properties of OC and OC–Zn hydrogels and their effects on the osteogenic differentiation of hPDLSCs. As shown in Fig. 6A, zinc-based hydrogels significantly increased the expression level of ALP compared with the blank control group. However, with the increase in zinc ion concentration, the cell viability of hPDLSCs decreased. Among them, OC–Zn3 has been shown to maintain the survival rate and osteogenic differentiation of hPDLSCs. As can be seen from ARS images, OC–Zn3 significantly promoted the mineralization of osteogenic differentiated hPDLSCs, which further confirms the osteogenic efficacy of zinc-containing hydrogel.[43,44]

Materials and methods

Materials

Sodium hyaluronate (HA, molecular weight 40–80 kDa), sodium (meta) periodate and glycol were purchased from Aladdin Biochemical Technology Co. Ltd (Shanghai, China). Carboxymethyl chitosan (CMCS) was purchased from Solarbio® Life Sciences. All the chemicals were used without further purification.

Synthesis and characterization of oxidized hyaluronate (OHA)

HA (1 g) was first dissolved in deionized water to obtain 1.0% w/v solution. Then, 10 mL of sodium (meta) periodate aqueous solution (0.5 M) was added dropwise to the solution. The reaction was stirred vigorously in the dark at room temperature for 24 h (as the sodium meta periodate is light sensitive).[13,45] The reaction was terminated by adding glycol (0.05% v/v) and kept for 1 h. Afterward, the oxidized HA solution was dialyzed against deionized water for 72 h (molecular weight cutoff 3500 D, Solarbio® Life Sciences). Samples were frozen and lyophilized in a freezer and stored at 4 °C until further processing. The formation of aldehyde functional groups was confirmed by using Attenuated Total Reflectance Fourier transformed Infrared Spectroscopy (ATR-FTIR, Nicolet iN10 FTIR spectrometer in the 400–4000 cm^{-1}, Thermo Fisher Scientific, Waltham, MA, USA). Proton nuclear magnetic resonance (^1H NMR, Bruker Advance III, Germany) measurement was performed to further validate the successful OHA and the degree of modification.

Preparation of oxidized hyaluronate (OHA)/carboxymethyl chitosan (OC) and $ZnCl_2$ cross-linked OC–Zn hydrogel

OHA was dissolved in deionized water to a final concentration of 5% (w/v). CMCS was dissolved in deionized water to obtain the final concentration of 3% (w/v). The above solutions were blended in equal volumes to prepare the OC hydrogel. To endow the self-healing hydrogels with more antibacterial and osteogenic functions, a certain amount of $ZnCl_2$ was dissolved in the OHA solution. The final concentration of $ZnCl_2$ in the hydrogel was 0.03, 0.06, and 0.12% (w/v), respectively. These three hydrogels are named OC–Zn3, OC–Zn6, and OC–Zn12.

Characterization of the hydrogels

Gelation time test. The gelation time at 37 °C was determined by the tilt method.[46,47] Equal volumes of OHA and CMCS solutions were mixed in a vial. The time when the liquid did not flow in the inverted vial was recorded as the gelation time ($n = 3$).

FTIR analysis. ATR-FTIR was used to characterize the OC and OC–Zn hydrogels to confirm the interaction among CMCS, OHA, and $ZnCl_2$. The FTIR spectra were recorded in the wavenumber region of 4000–400 cm^{-1} at 25 °C using the dried hydrogel samples.

Micromorphology. The morphology of the dried hydrogel samples was observed using scanning electron microscopy (SEM, TESCAN VEGA3, Czech).

Rheological analysis. A TA rheometer (DHR-2) was employed to test the rheological properties of these hydrogels. 500 μL of hydrogel disk was placed between the parallel plates of 20 mm diameter.

Self-healing experiment. The self-repairing behavior of the samples was evaluated by macroscopic observation. First, two sample plates stretched with red and green dyes were cut into halves. Then, two semicircles of different colors were put together at room temperature for 20 min.

Swelling ratio (SR) and stability. The swelling behavior was evaluated by measuring the mass difference before and after incubation of the hydrogel samples in PBS solution (0.1 M, PH 7.4).[48,49] In brief, the dry hydrogels weighted W_d were immersed into 30 mL of PBS in the sealed vials at 37 °C. And then at a predetermined time point, the samples were taken out and the residual liquid on the hydrogel surface was carefully wiped off with filter paper. The swelled samples were weighed (W_s) and subsequently put back into the same vial. Samples were used in triplicate. The SR of the samples was calculated according to the following formula (1):

$$\mathrm{SR} = \frac{W_s - W_d}{W_d} \times 100\% \quad (1)$$

Cell culture. Human periodontal ligament stem cells (hPDLSCs) were obtained according to previous studies.[50] hPDLSCs from the periodontal ligament of healthy third molars without any dental and periodontal tissue disease. The third molars used were all from patients (18–25 years old) without systemic diseases. All the patients came to Qingdao Stomatological Hospital for oral and maxillofacial surgery and signed the informed consent. hPDLSCs were extracted from tissue blocks, and the 3–6 generations of hPDLSCs were used in this study. According to different experiments, different concentrations of fetal bovine serum (FBS, Procell, Wuhan, China) and 1% penicillin–streptomycin were added into α-MEM medium (Biological Industries, Israel) to culture hPDLSCs. All cells were cultured at 37 °C, 5% CO_2 under constant humidity conditions.

Hemolysis analysis. The hemolytic activity of hydrogels was measured by a direct contact method in reference to previous studies.[47,51] Whole human blood was selected to assess the hemolysis of samples. Anticoagulated human blood (1 mL) was diluted with 5 mL of normal saline (NS). NS (1 mL)-containing different specimens (20 mg) were prepared at 37 °C. Then 200 μL of diluted blood was added into 1 mL of (i) the sample suspensions; (ii) 1 mL of NS, the negative control; and (iii) 1 mL of Triton X-100, the positive control. The above solutions were incubated at 37 °C for 1 h, and then centrifuged at 1500 rpm for 5 min. The supernatants in all groups were carefully transferred to the 96-well plate, and the optical density (OD) values were analyzed at 540 nm. Each group was repeated in triplicate. The hemolysis ratio (HR) was calculated according to the formula (2):

$$\mathrm{HR}\% = \frac{\mathrm{OD}_{\mathrm{specimen}} - \mathrm{OD}_{\mathrm{negative}}}{\mathrm{OD}_{\mathrm{positive}} - \mathrm{OD}_{\mathrm{negative}}} \times 100\% \quad (2)$$

Cell viability assay. The cell viability and proliferation were quantitatively analyzed by Cell Counting Kit-8 (CCK-8; Absin Bioscience Inc., Shanghai, China). Briefly, hPDLSCs from passages 3 to 5 were seeded into 96-well plates at an initial concentration of 5×10^3 cells per well and cultured in a humidified incubator containing 5% CO_2 at 37 °C for 24 h. The culture medium was replaced by the extract solutions (the hydrogels were prepared and washed with sterile PBS three times to remove any uncross-linked pregel solution and ensure the pH balance. Then, 3 mL of culture medium was co-incubated with hydrogel samples (220 μL) with overnight shaking at 37 °C). After culturing for 1, 3, and 5 days, the cells were incubated with medium containing the CCK-8 reagent (10%) for 2 h, and the absorbance of the medium at 450 nm was detected by a microplate reader (800TS, Bio-Tek, China). Cells seeded on plates without extract solutions and pristine were used as the control group and the blank group, respectively. The equation for calculating the cell viability is as follows (3):

$$\text{Cell viability} = \frac{\mathrm{OD}_{\mathrm{samples}} - \mathrm{OD}_{\mathrm{blank}}}{\mathrm{OD}_{\mathrm{control}} - \mathrm{OD}_{\mathrm{blank}}} \times 100\% \quad (3)$$

Cell adhesion performance. After being co-cultured with different concentrations of sample solutions in 24-well plates at a concentration of fifty thousand cells per well, the hPDLSCs were fixed with 4% paraformaldehyde for 20 min and treated with 0.5% Triton X-100 for 3 min. Then, the cells were stained with TRITC-Phalloidin and DAPI for the cytoskeleton and nucleus according to the manufacturer's instructions. The different images of the cells were captured *via* inverted fluorescence microscopy (Nikon A1 MP, Japan).

Culture of bacteria and their biofilms. *Fusobacterium nucleatum* (*F. nucleatum*) and *Staphylococcus aureus* (*S. aureus*) were used as Gram-negative and Gram-positive bacteria, respectively, to evaluate the antibacterial and antibiofilm performance of the hydrogel.[52] The frozen bacteria were activated in Tryptic Soy Broth (TSB) medium and quadrant-streaked on an agar plate. A single bacteria colony on the agar growth plate was isolated and cultured with 10 mL of TSB in an orbital shaker (BHWY-200, Saifu, China) overnight at 37 °C. The bacterial suspension was diluted with TSB media to obtain the fixed OD600 value of ~0.05 (approximately equal to 10^8 colony-forming units (CFU) mL^{-1}) for further use. To obtain the biofilm, 500 μL of *F. nucleatum* suspension (1×10^8 CFU mL^{-1}) was dripped into a 24-well plate

(with 14 mm diameter glass coverslips) and incubated in a biochemical incubator (SPX-150, Saifu, China) for 48 h. After discarding the medium carefully and gently, a visible performed biofilm was observed on the glass coverslips. Then the biofilm was washed with normal saline three times slower to remove the planktonic bacteria for subsequent experiments.

Anti-*F. nucleatum* and *S. aureus* test. The antimicrobial experiments were carried out by co-culture of bacterial suspension with hydrogels. The hydrogels were prepared and washed with sterile PBS three times to remove any uncross-linked pregel solution and ensure the pH balance. Then, 3 mL of bacterial suspension was co-incubated with hydrogel samples (220 μL) with overnight shaking at 37 °C. Commercially available minocycline (5 mg) served as a positive control group. After that, 20 μL of the gradient-diluted bacterial suspensions were spread evenly on the agar plates at 0, 0.5, 1, 2, 3, 4, 6, 8, 12 and 24 hours. These plates were incubated for 24 h in a biochemical incubator at 37 °C, and the number of colonies was counted. TSB medium co-cultured with bacterial suspensions as the negative control group. Tests were repeated five times for each group, and the results were described as bacterial kill%:

$$\text{Bacterial kill\%} = \frac{\text{CFU}_0 - \text{CFU}_1}{\text{CFU}_0} \times 100\% \quad (4)$$

where CFU_0 and CFU_1 are the number of bacteria colonies per milliliter on the agar plate without any treatment and experimental groups, respectively.

Morphological changes of *F. nucleatum* and *S. aureus*. The morphology of bacterial morphology and the integrities of the bacterial membrane after different treatments were also observed by TEM. In short, the blank, OC–Zn12 groups were co-cultured with bacterial suspensions for 20 h. Then they were centrifuged at 8000 rpm for 5 min, washed three times with PBS, and fixed with 2.5% glutaraldehyde. 200 μL of bacterial suspension was observed by TEM.

Antibiofilm tests. Firstly, the biofilms treated with the hydrogels (1 mL) were examined by crystal violet (CV) staining. Each group was added with 300 μL of 0.1% CV solution, incubated at room temperature for 15 min, and then gently and slowly washed with PBS. Then, anhydrous ethanol was added and treated for 15 min. The absorbance at 570 nm was recorded with a microplate reader (Bio-TEK, USA). Subsequently, hydrogels of different concentrations of $ZnCl_2$ were added into the 24-well plate in which biofilm had formed and co-cultured for 12 h. The biofilm formed on the coverslips was stained with the LIVE/DEAD BacLight™ Bacterial Viability Kit. The fluorescence intensity of the biofilm was observed using a confocal laser scanning microscope (CLSM, Leica TCS SP8, Germany).

***In vitro* osteogenic differentiation.** To evaluate the osteoinductive property of the hydrogels, the PDLSCs were first seeded in 6-well plates. When they reached 90% confluence, the culture medium was replaced with extracts of hydrogels. Alkaline phosphatase (ALP) activity and Alizarin Red Staining (ARS) were performed to evaluate the osteogenic potential. ALP activity assay and NBT/BCIP ALP staining kits (Beyotime Biotechnology, China) were used to analyze the ALP activity according to the manufacturer's instructions on day 7. For ARS staining, 10% ARS solution (Sigma-Aldrich) was used to stain cells on day 21 for 5 min and washed with water.

Statistical analysis. All values are expressed as mean ± standard deviation (mean ± SD). Graphpad Prism 9.0 was used to calculate data and measure differences between the experimental groups using Student's *t*-test, one-way and two-way ANOVA tests followed by a Tukey post hoc test for pairwise comparison. A value of $p \leq 0.05$ was considered statistically significant.

Conclusion

In summary, OC–Zn hydrogels were successfully designed and prepared in this study. The formation of dynamic Schiff base (imine) bonds between –CHO in OHA and $–NH_2$ in CMCS, and dynamic coordination bonds between COO-, $–NH_2$, and –OH in polysaccharides and Zn^{2+} constitute a dynamic network that forms injectable and self-healing hydrogels. The hydrogels exhibited rapid gelation and shear thinning, which contributed to their injectability, as well as rapid and reproducible self-healing properties. In addition, tunable mechanical and swelling degradation was achieved by adding different concentrations of Zn^{2+} to form different ratios of bi-dynamic bonds. The addition of zinc ions enhanced the antimicrobial properties of the hydrogel while conferring satisfactory osteogenic activity to the hydrogel (OC–Zn3). The developed hydrogel has great potential as a drug delivery system for periodontitis.

Author contributions

Yuhan Liu: supervision, methodology, writing – review & editing; Mei Yang: conceptualization, methodology, investigation, software, writing – original draft; Yuanping Hao: software; Dejiang Du: methodology. Haiyu Zhang: investigation, methodology. All authors have read and approved the manuscript.

Conflicts of interest

The authors declare no conflicts of interest.

Acknowledgements

This research was financially supported by Qingdao South District Science and Technology Planning Project (Grant No. 2022-2-019-YY), the Qingdao Key Health Discipline Development Fund (2022–2024), Qingdao Clinical Research Center for Oral Diseases (Grant No. 22-3-7-lczx-7-nsh), Shandong Provincial Key Medical and Health Discipline of Oral Medicine (Qingdao University Affiliated Qingdao Stomatological Hospital) (2024–2026), and the Doctor Fund Project of Qingdao Stomatological Hospital (2023QN07).

References

1 G. C. Armitage, *Periodontology 2000*, 2004, **34**, 9–21.
2 G. Hajishengallis and T. Chavakis, *Nat. Rev. Immunol.*, 2021, **21**, 426–440.

3 R. J. Genco and M. Sanz, *Periodontology 2000*, 2020, **83**, 7–13.
4 D. Herrera, P. Matesanz, C. Martín, V. Oud, M. Feres and W. Teughels, *J. Clin. Periodontol.*, 2020, **47**, 239–256.
5 F. Graziani, D. Karapetsa, B. Alonso and D. Herrera, *Periodontology 2000*, 2017, **75**, 152–188.
6 R. G. Caffesse, P. L. Sweeney and B. A. Smith, *J. Clin. Periodontol.*, 1986, **13**, 205–210.
7 R. S. Wilder and K. S. Bray, *Periodontology 2000*, 2016, **71**, 65–81.
8 X. Tan, S. Liu, X. Hu, R. Zhang, X. Su, R. Qian, Y. Mai, Z. Xu, W. Jing, W. Tian and L. Xie, *ACS Appl. Mater. Interfaces*, 2023, **15**, 391–406.
9 Y. Tang, Q.-X. Huang, D.-W. Zheng, Y. Chen, L. Ma, C. Huang and X.-Z. Zhang, *Mater. Today*, 2022, **53**, 71–83.
10 Y. Yin, S. Yang, D. Ai, H. Qin, Y. Sun, X. Xia, X. Xu, W. Ji and J. Song, *Adv. Funct. Mater.*, 2023, **33**, 2301062.
11 X. Zhao, Y. Yang, J. Yu, R. Ding, D. Pei, Y. Zhang, G. He, Y. Cheng and A. Li, *Biomaterials*, 2022, **282**, 121387.
12 S. Liu, Y.-N. Wang, L. Yu, J. Li and S. Ge, *Chem. Eng. J.*, 2022, **432**, 134308.
13 H. Guo, S. Huang, X. Yang, J. Wu, T. B. Kirk, J. Xu, A. Xu and W. Xue, *ACS Appl. Mater. Interfaces*, 2021, **13**, 61638–61652.
14 Z. Yu, Q. Li, X. He, X. Wang, Y. Wen, L. Zeng, W. Yu, P. Hu and H. Chen, *Eur. Polym. J.*, 2023, **197**, 112330.
15 S. Li, M. Pei, T. Wan, H. Yang, S. Gu, Y. Tao, X. Liu, Y. Zhou, W. Xu and P. Xiao, *Carbohydr. Polym.*, 2020, **250**, 116922.
16 P. Bertsch, M. Diba, D. J. Mooney and S. C. G. Leeuwenburgh, *Chem. Rev.*, 2023, **123**, 834–873.
17 B. D. Zheng, J. Ye, Y. C. Yang, Y. Y. Huang and M. T. Xiao, *Carbohydr. Polym.*, 2022, **275**, 118770.
18 Z. Zou, Z. Zhang, H. Ren, X. Cheng, X. Chen and C. He, *Biomaterials*, 2023, **301**, 122251.
19 Y. Pang, H. Wang, Y. Yao, D. Chen, R. Yang, Z. Wang, J. Yang, Y. Li and W. Liu, *Adv. Funct. Mater.*, 2023, **33**, 2303095.
20 S. H. Lin, A. P. H. Huang and S. h. Hsu, *Adv. Funct. Mater.*, 2023, **33**, 2303853.
21 A. Moeini, P. Pedram, P. Makvandi, M. Malinconico and G. Gomez d'Ayala, *Carbohydr. Polym.*, 2020, **233**, 115839.
22 Y. Hao, W. Zhao, H. Zhang, W. Zheng and Q. Zhou, *Carbohydr. Polym.*, 2022, **287**, 119336.
23 H. Weng, W. Jia, M. Li and Z. Chen, *Carbohydr. Polym.*, 2022, **294**, 119767.
24 Y. Lin, J. Xu, Y. Dong, Y. Wang, C. Yu, Y. Li, C. Zhang, Q. Chen, S. Chen and Q. Peng, *Carbohydr. Polym.*, 2023, **314**, 120962.
25 N. Mutlu, L. Liverani, F. Kurtuldu, D. Galusek and A. R. Boccaccini, *Int. J. Biol. Macromol.*, 2022, **213**, 845–857.
26 T. Khodaei, J. Nourmohammadi, A. Ghaee and Z. Khodaii, *Carbohydr. Polym.*, 2023, **302**, 120371.
27 C. Zhou, Y. Zou, R. Xu, X. Han, Z. Xiang, H. Guo, X. Li, J. Liang, X. Zhang, Y. Fan and Y. Sun, *Mater. Horiz.*, 2023, **10**, 3114–3123.
28 X. Yin, Y. Hao, Y. Lu, D. Zhang, Y. Zhao, L. Mei, K. Sui, Q. Zhou and J. Hu, *Adv. Funct. Mater.*, 2021, **31**, 2105614.
29 J. Xing, Y. Ding, X. Zheng, P. Yu, M. Qin, R. Qiu, Y. Li, S. Shang, J. Xie and J. Li, *Chem. Eng. J.*, 2022, **444**, 136580.
30 K. Yang, X. Zhou, Z. Li, Z. Wang, Y. Luo, L. Deng and D. He, *ACS Appl. Mater. Interfaces*, 2022, **14**, 43010–43025.
31 J. Wang, H. Cheng, W. Chen, P. Han, X. Yao, B. Tang, W. Duan, P. Li, X. Wei, P. K. Chu and X. Zhang, *Chem. Eng. J.*, 2023, **452**, 139474.
32 Y. Xin, Z. Guo, A. Ma, E. Shi, Z. Li, Z. Liang, Z. Qian, L. Yang, Y. Wang, M. Cao and X. Yang, *Chem. Eng. J.*, 2023, **451**, 138782.
33 Y. Tian, Y. Li, J. Liu, Y. Lin, J. Jiao, B. Chen, W. Wang, S. Wu and C. Li, *Bioact. Mater.*, 2022, **9**, 428–445.
34 N. Mukherjee, S. Ghosh, J. Sarkar, R. Roy, D. Nandi and S. Ghosh, *ACS Appl. Mater. Interfaces*, 2023, **15**, 33457–33479.
35 L. Yang, Z. Han, C. Chen, Z. Li, S. Yu, Y. Qu and R. Zeng, *Mater. Sci. Eng., C*, 2020, **117**, 111265.
36 W. Tan, T. Long, Y. Wan, B. Li, Z. Xu, L. Zhao, C. Mu, L. Ge and D. Li, *Carbohydr. Polym.*, 2023, **312**, 120824.
37 A. Sirelkhatim, S. Mahmud, A. Seeni, N. H. M. Kaus, L. C. Ann, S. K. M. Bakhori, H. Hasan and D. Mohamad, *Nano-Micro Lett.*, 2015, **7**, 219–242.
38 L. E. Shi, Z. H. Li, W. Zheng, Y. F. Zhao, Y. F. Jin and Z. X. Tang, *Food Addit. Contam. Part A Chem. Anal. Control Expo. Risk Assess.*, 2014, **31**, 173–186.
39 X. Zhu, C. Liang, J. Chen, J. Gao, W. Chen, Q. Ouyang, L. Luo, Z. Huang, H. Luo, L. Chen and J. Chen, *Chem. Eng. J.*, 2024, **481**, 148136.
40 Y. Sheng, Z. Chen, W. Wu and Y. Lu, *Drug Discovery Today*, 2023, **28**, 103455.
41 B. P. Lima, L. I. Hu, G. W. Vreeman, D. B. Weibel and R. Lux, *Microb. Ecol.*, 2019, **78**, 336–347.
42 A. Adak, S. Ghosh, V. Gupta and S. Ghosh, *Biomacromolecules*, 2019, **20**, 1889–1898.
43 T. Lu, J. Zhang, X. Yuan, C. Tang, X. Wang, Y. Zhang, K. Xiong and J. Ye, *Mater. Sci. Eng. C.*, 2021, **131**, 112490.
44 Y. Zhao, J. Li, L. Liu, Y. Wang, Y. Ju, C. Zeng, Z. Lu, D. Xie and J. Guo, *Adv. Healthcare Mater.*, 2023, **12**, 2300303.
45 Y. Xu, R. Rothe, D. Voigt, S. Hauser, M. Cui, T. Miyagawa, M. Patino Gaillez, T. Kurth, M. Bornhauser, J. Pietzsch and Y. Zhang, *Nat. Commun.*, 2021, **12**, 2407.
46 M. Wang, S. Lin, M. Liu, J. Jiao, H. Mi, J. Sun, Y. Liu, R. Guo, S. Liu, H. Fu, Y. Yang and R. Li, *Chem. Eng. J.*, 2023, **463**, 142283.
47 Y. Hao, C. Yuan, J. Deng, W. Zheng, Y. Ji and Q. Zhou, *ACS Appl. Mater. Interfaces*, 2022, **14**, 16006–16017.
48 Z. Zhou, J. Xiao, S. Guan, Z. Geng, R. Zhao and B. Gao, *Carbohydr. Polym.*, 2022, **285**, 119235.
49 Z. Ahmadian, A. Correia, M. Hasany, P. Figueiredo, F. Dobakhti, M. R. Eskandari, S. H. Hosseini, R. Abiri, S. Khorshid, J. Hirvonen, H. A. Santos and M. A. Shahbazi, *Adv. Healthcare Mater.*, 2021, **10**, e2001122.
50 J. Yu, X. Wu, W. Zhang, F. Chu, Q. Zhang, M. Gao, Y. Xu and Y. Wu, *Hum. Cell*, 2023, **36**, 1389–1402.
51 M. Liu, L. Huang, X. Xu, X. Wei, X. Yang, X. Li, B. Wang, Y. Xu, L. Li and Z. Yang, *ACS Nano*, 2022, **16**, 9479–9497.
52 A. Adak, V. Castelletto, A. de Sousa, K.-A. Karatzas, C. Wilkinson, N. Khunti, J. Seitsonen and I. W. Hamley, *Biomacromolecules*, 2024, **25**, 1205–1213.